Discover Applied Sciences

Research

Assessment of blended cement containing waste basalt powder: physicomechanical and electrochemical impedance spectroscopy investigations

Israa A. Abo Hashem[1] · Ghalia A. Gaber[1] · Amal S. I. Ahmed[1] · Nabil A. Abdel Ghany[2]

Received: 12 September 2023 / Accepted: 1 July 2024
Published online: 16 July 2024

Abstract
Basalt powder (BP) is the residue of a plant that crushes basalt stones. This work deals with the effect of waste BP on the properties of cement mortars and the physical properties of hardened mortars. Modified concrete was prepared by partial replacement of BP in amount of 5, 10, 20% by weight of cement. Physico-mechanical properties and corrosion resistance were investigated. Electrochemical impedance spectroscopy (EIS) was used to examine the corrosion behavior of cement pastes with a partial addition of basalt powder in aggressive solutions of 5% NaCl and 5% $MgCl_2$ for up to 270 days. Infrared spectroscopy (IR), X-ray diffraction (XRD), scanning electron microscopy (SEM) and energy-dispersive X-ray spectroscopy (EDX) were also performed to investigate the hydration process and microstructure formation of the basalt blended paste. Results indicate that the addition of basalt powder as a partial replacement of cement influences the microstructure of the interfacial transition zone (ITZ), which is denser and stronger than in cement paste without basalt powder. The filler effect of the basalt powder improves the compressive strength of cement paste. Also, comparing BP0 and BP20 in 5% NaCl after 270 days, the partial substitution of cement with BP resulted in a higher compressive strength of 671 and 895 kg/cm^2, respectively. The EIS results also showed the highest values of R_p 953 ohms cm^2 after 270 days. This high corrosion resistance might indicate the binding by high Al_2O_3 that reduced the free aggressive chloride ions in the solution.

Article Highlights

- The addition of basalt powder as a partial replacement of cement, improved the compressive strength of the concrete.
- The physicochemical and mechanical investigations showed that the basalt addition led to physical densification and more ITZ robust of cement matrix.
- EIS measurements showed that BP20 sample in 5% NaCl had a high R_p, 953 ohms cm^2 after 270 days indicated higher corrosion resistance.

Keywords Basalt powder · Portland cement · Compressive strength · Corrosion behavior · Aggressive media

✉ Nabil A. Abdel Ghany, na.abdelghany@nrc.sci.eg; na_manakhly@yahoo.co.uk | [1]Department of Chemistry, Faculty of Science (Girls), Al-Azhar University, Yousef Abbas Str., P.O. Box: 11754, Nasr City, Cairo, Egypt. [2]Physical Chemistry Department, Electrochemistry and Corrosion Lab, National Research Centre, Dokki, Cairo 12622, Egypt.

1 Introduction

Cement production is one of the sectors that produces a lot of carbon dioxide; for each tone of Portland cement clinker produced, around another tone of carbon dioxide is released [1]. Supplementary cementitious materials (SCMs) are finely ground pozzolanic materials that are used to replace part (or whole) of the OPC in a concrete mixture to embellish its fresh and hardened properties [2, 3]. These materials react chemically with hydrating cement to form a modified paste microstructure. SCMs possess high pozzolanic or latent hydraulic reactivity [4]. Pozzolana is a siliceous material that is capable of reacting with lime, $Ca(OH)_2$, in the presence of water to form cementitious compounds (as C–S–H gel) [5, 6]. Nowadays, different types of mineral admixtures are added to Portland clinker during the milling process or directly to the cement. The pozzolanic materials used in the cement industry, include pozzolanic, autopozzolanic, and crystalline materials, some of which interact physically and/or chemically with Portland cement or its hydration products [7–10].

Ghanem et al. [11] investigated the impact of different percentages of metakaolin (MK) cement replacement on the corrosion behaviour of implanted reinforcing steel bars. The corrosion behaviour of the reinforcing steel in cement in a 3.5% NaCl solution is found to be improved by the use of metakaolin as a 20% w/w cement replacement. The recommended ratio to minimize the corrosion rate is nearly 5% MK replacement in 5% $MgSO_4$ solution.

By measuring the bulk density, total porosity, and compressive strength for up to 90 days, the impact of a 5% $NaSO_4$ solution on slag cement was investigated by Ahmed et al. [12]. The findings indicated that the presence of sodium cations has a negative effect. This is primarily caused by the interaction between the Na^+ ion and the cement matrix CSH. Additionally, the aggressive media has a negative impact on how well all forms of cement hydrate. Ordinary Portland cement was also negatively impacted more than other forms of cement.

Crystallinity, chemical composition, specific surface area and particle size distribution are some of the variables that affect the mineral admixtures' function in blended cement and concrete. Mineral admixtures are frequently used in concrete to enhance its chemical, physical and mechanical characteristics, in addition to reducing and conserving energy consumption. The variables contributing to deteriorating concrete durability may be decreased, or its resistance to sulphate attack may be enhanced, by utilizing cement replacement materials [13].

The traditional way of designing concrete based on strength has changed due to increasing durability requirements. The strength of the interfacial transition zone is significantly reduced by the differences in aggregate and mortar elastic modulus, linear expansion coefficient, and other characteristics. In this case, dangerous ions could readily permeate the concrete and cause the steel to corrode, which reduces its durability even further [14, 15].

Various substances, including basalt powder (BP), were employed to prevent this inherent flaw. The research on basalt materials in cement-based materials focuses primarily on macro properties, lacking a deep explanation of the influence of their surface chemical properties on cement-based materials [16, 17]. BP is produced in large quantities around the world as a by-product, causing serious environmental pollution and health risks. The use of mineral dust as an admixture can contribute to solving these problems [18–20]. BP is believed to be a mineral with a large specific surface area and high SiO_2 and Al_2O_3 contents and can be used as a supplementary cementing material [21]. Tasong et al. [22] studied the interaction between BP and ions in a cement solution. BP absorbed a large amount of hydroxide, sulphate, calcium, and potassium ions and dissociated a large amount of silicate and alumina ions. This indicated that there is a distinct chemical interaction on its surface. Liu et al. [23] found that BP has a retardation effect on cement hydration. Li et al. [24] used 15% BP to replace cement to prepare UHPC with different curing conditions. The results showed that the strength of basalt concrete is 10.3% lower than that of reference concrete at ambient temperature, while that of basalt concrete is 10.8% and 7.3% higher than that of reference concrete under steam curing and autoclave curing, respectively. Saraya [5] also found that the pozzolanic reaction of BP was weak before 28 d. Youness et al. [25] found that adding BP reduces the fluidity of cement-based materials. It was proposed that the decline in flow ability of the mixed paste was caused by its sharp and rough surface.

Additionally, by saturating the pores and changing their diameter and distribution, mineral additions have increased their strength. In the early history of the Earth, basalt, a form of volcanic rock, was produced as cooled magma. The bulk of igneous minerals is found in an active state and undergoes physical or chemical weathering in the environment to become more stable clay minerals. [26]. Previous studies that examined wastes found that fine powder might improve the compressive strength and physicomechanical characteristics of concrete [27]. The current work intends to assess and evaluate the physicomechanical properties and corrosion using electrochemical impedance spectroscopy of cement pastes replaced with different ratios of basalt powder. The study was conducted in different aggressive media (5%NaCl and 5% $MgCl_2$) for up to 270 days to assess the characteristics of cement pastes and the protection of reinforcing steel.

Table 1 Chemical composition of (OPC) and (BP)

Oxides Formula	OPC Conc., %	BP Conc., %	Oxides Formula	OPC Conc., %	BP Conc., %
SiO_2	20.961	51.241	Al_2O_3	5.764	16.635
ZrO_2	–	0.011	MgO	0.667	4.462
MnO	0.124	0.292	K_2O	0.212	0.790
SO_3	4.824	0.082	ZnO	0.022	0.011
TiO_2	0.313	1.638	SrO	0.099	0.046
Na_2O	0.889	3.741	ZrO_2	0.022	0.029
CaO	58.424	6.768	BaO	0.022	0.056
Fe_2O_3	4.976	11.730	Cl	0.191	0.043
P_2O_5	0.116	0.685	LOI	2.400	1.750

Table 2 Mix composition of the cements paste, (wt. %)

Mix No	OPC	Basalt Powder
BP0	100	0
BP5	95	5
BP10	90	10
BP20	80	20

The results of this study might contribute to gaining a deeper understanding of the influence of basalt materials on the properties of cement-based materials and provide theoretical support for better use of BP in cement-based materials to reduce carbon emissions and environmental pollution.

2 Experimental

2.1 Materials

Tourah Ordinary Portland Cement, CEM I 42.5 N (OPC), was used as a material in this study, and basalt powder (BP) was produced from Aswan quarries (Egypt). The chemical analyses of (OPC) and (BP) are depicted in Table 1. The specific gravity at 20 °C of BP is 2.9661 and 3.15 for OPC.

2.2 Preparation of cement pastes

In the beginning, when a cement weight was applied to a seamless, impermeable surface, a crater was created. With the aid of a trowel, the crater was filled with the required amount of mixing water as shown in Table 2 (Cement pastes were prepared with a standard water-to-cement ratio of ASTM C 187-04). The water/cement ratio was maintained constant at 0.3 parts water per parts cement by weight this mean that for every 1 KG of cement needs approximately 0.3 L of water. After being gently toweled to take up the water for about a minute, the dry cement was thoroughly mixed vigorously and continuously for approximately three minutes manually. After the top layer had been compacted, the mould was filled with cement paste. And left there until a homogeneous specimen was created. Using an edgeless trowel, the top of the paste was smoothed off and brought level with the top of the mould. These percentages were substituted for the dry cement weight after mixing cement with tap water to make pastes of 5, 10, and 20% basalt powder additions. After adding and thoroughly combining basalt powder, the mixture was used with the mould. Moulding samples were immediately dried in a humidifier at an ambient temperature for 24 h. When the moist curing time had ended, de-moulded cubes were used, and curing was continued underwater for the needed time of testing. Then the samples were subjected to aggressive medium, the cube 2.5 cm (1 inch-sides length) was de-moulded and curried underwater for about 28 days, in different solutions (5% NaCl and 5% $MgCl_2$) as shown in Fig. 1. Samples were investigated at specified intervals up to 9 months.

Fig. 1 Cubes immersed in 5%$MgCl_2$ and BP as raw material

2.3 Preparation of reinforcing steel for EIS

High-tensile steel bars (reinforcing steel 38), measuring 12 mm in diameter and 100 mm in height, were the reinforcing steel employed in this test. The surface of the rods was mechanically cleaned to remove the heavily adhered mill scales and cleaned with bi-distilled water, dried with acetone, and then covered in epoxy, while 1 cm^2 was not coated. The coating with cement pastes was used with steel reinforcement in a mouldier (cylindrical) with a 6 cm width and a 10 cm length, as shown in Fig. 2 and Table 3 which tabulated the chemical compositions of reinforcing steel.

2.4 Physico-mechanical investigations

2.4.1 Bulk density

Bulk density is defined as the mass of the dry solids divided by the total volume of the entire wet sample. By dividing the mass of dry cement particles by the volume of the cement sample, the bulk density can be calculated from Eq. 1 [28].

$$\text{Bulk density g/cm}^3 = M_d/V \quad (1)$$

where M_d is the mass of the dry cement sample (g) and V is the sum of the wet sample's volume (cm^3).

Each measurement was conducted on three equivalent individuals with the same preparation conditions and the average of the three results was calculated.

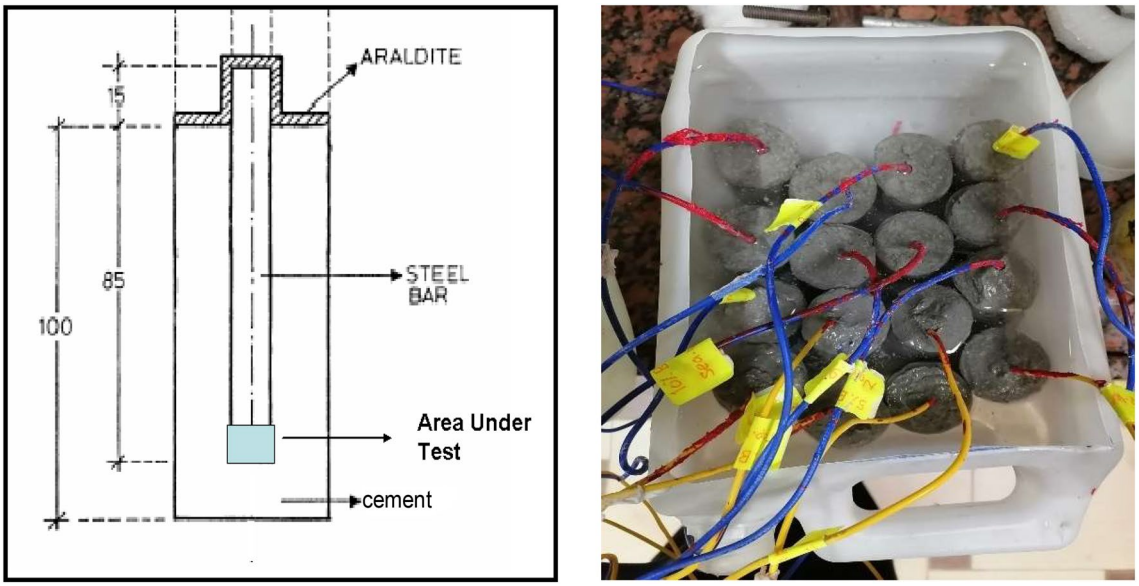

Fig. 2 Schematic representation of reinforcing steel in cement paste

Table 3 Chemical composition of reinforcing steel

Element	C	Si	Mn	P	S	Cr	Ni	Al	Fe
Wt %	0.323	0.169	0.782	0.032	0.019	0.0188	0.0135	0.033	98.58

2.4.2 Water absorption and total porosity

The water absorption was established according to Davraz et al. [29]. The Samples used were either boiled for five hours or submerged in water for 24 h. The water was then allowed to drain following the removal of the samples from it. Any apparent surface water was removed using a cloth that had been dampened. The samples' weight was recorded as saturated weight (Ws). The used samples were dried for one day at 80 °C in a ventilated oven. Dry weight (Wd), the final weight of the samples, was recorded. The water absorption percent is calculated from the following Eq. 2:

$$\text{Water absorption } \% = \left[\left(W_s - W_d\right)/W_d\right] \times 100 \tag{2}$$

The equation could be utilised to calculate the overall porosity of the cured cement pastes once the specimens' water absorption was established by Eq. 3:

$$\text{Total porosity } \% = W_s - W_d/\rho_w V \tag{3}$$

where ρ_w is the water density and V is the volume of the sample.

For each measurement, the average of the three measurements was calculated. Which was performed on three comparable specimens prepared under identical conditions?

2.4.3 Compressive strength

In order to assess compressive strength, 2.5 × 2.5 × 2.5 cm neat cement cubes were prepared, de-moulded, and constantly cured in a humidity chamber until the time of testing, as indicated in Fig. 3. For each assessment of compressive strength, a set of three cubes was used [30]. With a loading rate of 100 kg/min, compressive strength measurements were performed using two-ton Amsler testing equipment, according to Khater H.M. [31].

Fig. 3 Cubes in aggressive media, extracted and broken in a compressive strength machine

2.5 Characterization of hydrated paste mix design

2.5.1 Infrared spectroscopic

The fingerprint of the compound's infrared spectrum applies to both qualitative and quantitative examinations of the mixture. To be able to learn more about the hydrated products, IR spectral analysis was done on a sample of hydrated pastes. From the proper spectrum, it is occasionally feasible to draw inferences about structural elements. Alkali halide (KBr) pressed disc procedures are accustomed to preparing the samples because they further reduce IR scattering. 1.0 mg of the moist powder sample was mixed with 99 mg of potassium bromide in an agate mortar to form a homogeneous slurry. The mixture was compressed under a vacuum to provide a transparent disc with a diameter of 1.0 cm. Then, set the KBr disc in the spectrometer after moving it to a sample holder. The Jascoo FTIR 4600 was used to record the infrared spectrum analyses from KBr discs in the 400–4000 cm^{-1} range.

2.5.2 X-ray diffraction (XRD)

The sample being studied is placed into a high-energy beam of charged particles, such as electrons or protons, or an X-ray beam, to cause the release of distinctive X-rays. An atom in the sample has ground-state (or unexcited) electrons that are bonded to the nucleus at specific energy levels or shells when it is at rest. An electron's inner shell might be excited by the incident ray, ejecting the electron out of the shell and leaving an electron hole in its place. An electron from the outer, higher-energy shell then fills the hole, and the energy may result in the production of an X-ray. In the phase experiment, we used a Bruker D8 Discover with a Cu radiation source, a wavelength of 1.54 A, an applied voltage of 40 kV, and a filament current of 40 mA.

2.6 Electrochemical impedance spectroscopy

The Autolab 302N Potentiostat/Galvaniostat was accustomed to conducting electrochemical impedance investigations in a three-electrode system. The fundamental benefit of this strategy is that the electrode/electrolyte interface is represented by a completely electronic model. An electrical circuit with resistors and capacitors is frequently compared to an interface that is undergoing an electrochemical reaction. As a result, the equivalent circuit of an electrochemical system is a good fit. An impedance plot derived for a specific electrochemical system can be compared to one or more analogous circuits using AC (alternating current) circuit theory. The data is used to either confirm or, at the very least disprove, a mechanistic model for the system. Since the impedance data is revealed to be reliant on the disturbance signal amplitudes in the vicinity of 5 to 15 mV, a 10 mV amplitude signal is typically employed for impedance measurements. The typical working frequency range used was from 1 mHz to 100 kHz. Data generation processes, including collection, processing, storage, retrieval, and analysis, have been automated by Metrhom

Table 4 Bulk density (g/cm^3) of cement pastes as a function of curing time of various proportions of basalt powder in 5% NaCl solution

Mix No	Time (days)			
	Bulk density (g/cm^3)			
	28 Days	90 Days	180 Days	270 Days
BP0	1.94	1.96	1.97	1.99
BP5	2.01	2.02	2.03	2.05
BP10	2.04	2.06	2.07	2.08
BP20	2.05	2.07	2.08	2.10

Table 5 Bulk density (g/cm^3) of cement pastes as a function of curing time of various proportions of basalt powder in 5% $MgCl_2$ solution

Mix No	Time (days)			
	Bulk density (g/cm^3)			
	28 Days	90 Days	180 Days	270 Days
BP0	1.91	1.93	1.94	1.95
BP5	1.97	1.97	1.98	1.99
BP10	1.99	1.99	2.01	2.03
BP20	2.03	2.04	2.05	2.06

Nova 2.1.5 software. After initial setup measurements, the electrode impedance data may be collected over a wide frequency range (1 mHz–100 kHz).

2.7 Spectroscopic analysis

The surface morphology and grain size were observed using scanning electron microscopy (SEM). Energy dispersive X-ray analysis (EDX) was used to identify the constituents on the surface of reinforcing steel after curing in various corrosive media. The analysis was carried out using JEOL JSM 5410 (Japan).

3 Result and discussion

3.1 Physico-mechanical properties of different mix designs

The influence of aggressive attack (5% NaCl or 5% $MgCl_2$ solution) was studied on different mix designs of OPC and basalt powder pastes for up to 270 days. In the beginning, samples of hardened cement pastes were cured under tap water for up to 28 days (zero time), then immersed in an aggressive medium for up to 28, 90, 180, and 270 days.

3.1.1 Bulk density

The concrete structure's densification and mechanical qualities are enhanced due to the filling and nucleation effects of the basalt powder. Concrete with basalt powder had a denser interfacial transition zone than concrete without basalt. In order to increase the performance of concrete, basalt powder was used instead of fine aggregate. According to ASTM C140 [32], the values of the bulk density of various proportions of basalt powder cured in tap water for up to 28 days (zero time) and then immersed in a 5% NaCl or 5% $MgCl_2$ solutions for up to 270 days are given in Tables 4, 5. Based on the duration of the cure period, these results are also displayed in Fig. 4. The results show that basalt powder in varied quantities rises in bulk density. An increase in the number of products is the primary reason for the increase in bulk density that developed and precipitated in the pores that were initially filled with water [33].

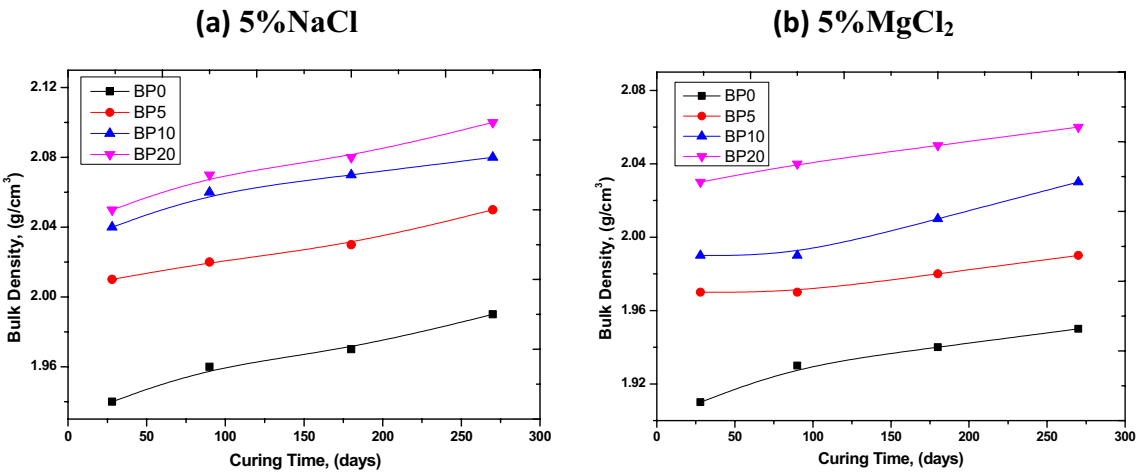

Fig. 4 Bulk Density (g/cm^3) of cement pastes as a function of curing time of various proportions of basalt powder in **a** 5%NaCl and **b** $MgCl_2$

Table 6 Water absorption (%) of cement pastes as a function of curing time of various proportions of basalt powder in 5% NaCl solution

Mix No	Time (days)			
	Water absorption, (%)			
	28 Days	90 Days	180 Days	270 Days
BP0	4.11	4.01	3.84	3.47
BP5	4.03	3.73	3.51	2.81
BP10	3.82	3.68	3.42	2.70
BP20	3.53	3.41	3.31	2.52

Table 7 Water absorption (%) of cement pastes as a function of curing time of various proportions of basalt powder in 5% $MgCl_2$ solution

Mix No	Time (days)			
	Water absorption, (%)			
	28 Days	90 Days	180 Days	270 Days
BP0	4.44	4.21	4.05	3.86
BP5	4.12	4.03	3.73	3.06
BP10	4.01	3.94	3.62	2.93
BP20	3.82	3.73	3.44	2.76

3.1.2 Water absorption

The values of water absorption of various proportions of basalt powder cured in tap water for up to 28 days (zero time) and then immersed in 5%NaCl or 5%$MgCl_2$ solutions for up to 270 days are given in Tables 6 and 7. Additionally, these are graphically depicted based on the length of the cure time in Fig. 5. With time, basalt powder absorbs less water in different proportions. This observation is explained by the fact that looks like small pozzolan particles block the capillary pore channels in cement paste, which results in a more even distribution of CSH gel and a reduction in pore structure and permeability voids [34].

3.1.3 Total porosity

Tables 8 and 9 provide the total porosity values for basalt powder in various proportions that have been cured in tap water for up to 28 days before being submerged in 5% sodium chloride or 5% magnesium chloride solutions for up to 270 days. In Fig. 6, these are also shown as a function of curing times. In plain cement (OPC) case pastes immersed in 5%

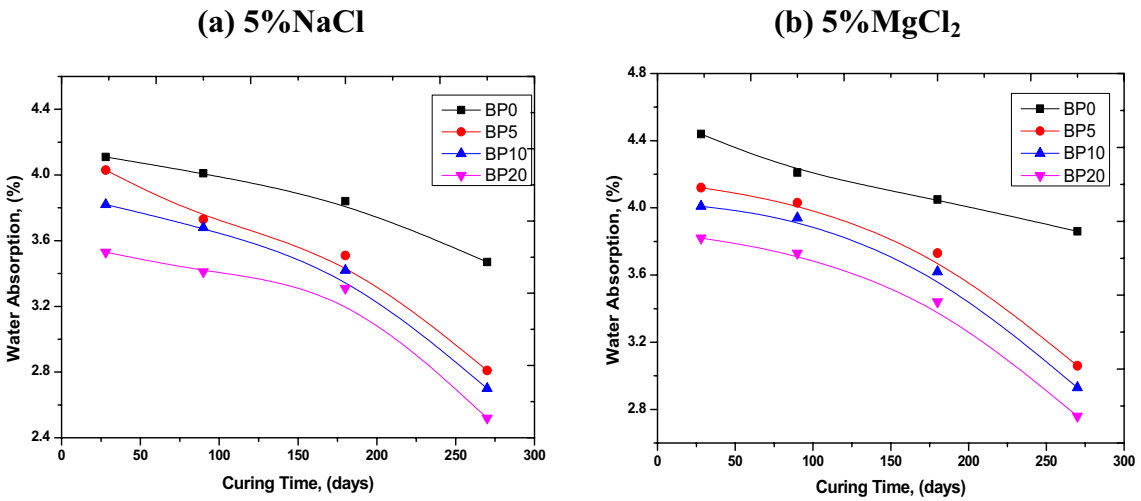

Fig. 5 Water Absorption(%) of cement pastes as a function of curing time of various proportions of basalt powder in **a** 5%NaCl and **b** $MgCl_2$

Table 8 Total porosity (%) of cement pastes as a function of curing time of various proportions of basalt powder in 5% NaCl solution

Mix No	Time (days)			
	Total porosity, (%)			
	28 Days	90 Days	180 Days	270 Days
BP0	24	23	22	19
BP5	23	22	19	18
BP10	21	19	18	16
BP20	18	17	16	14

Table 9 Total porosity (%) of cement pastes as a function of curing time of various proportions of basalt powder in 5% $MgCl_2$ solution

Mix No	Time (days)			
	Total porosity, (%)			
	28 Days	90 Days	180 Days	270 Days
BP0	27	25	24	22
BP5	25	23	21	20
BP10	23	22	20	19
BP20	21	19	18	17

NaCl or 5% $MgCl_2$ solutions, with longer cure times, the total porosity decreases. The precipitation of hydrated phases into the amorphous pores of cement pastes is the primary cause of porosity reductions. Due to the continuous hydration of cement compounds, hardened cement pastes' total pore volume decreases with curing time. The filling action of hydration products, which reduces pore volume, causes a decrease in total porosity.

According to the results, cement paste with basalt powder additives has a lower total porosity than paste without them. Total porosity is primarily determined by the size of capillary pores. However, it also has to perform with the size, distribution, shape, tortuosity, and continuity of the pores, in addition to the overall porosity of the material. The total porosity decreases when the content of fine pores increases and the content of larger capillary pores decreases. As a result, total porosity decreases with time and as the cement hydrates more or less. Basalt powders can reduce the overall porosity of cement paste, mostly due to physical dust interaction or, more specifically, their function as micro-fillers.

Basalt powder particles break the continuity of capillary pores and thereby contribute to the reduction of capillary water take and total porosity. With basalt powder additives, hetero nucleation significantly reduces cement paste's total porosity, which enhances the growth of crystallisation nuclei and the densification of cement paste. Due to the

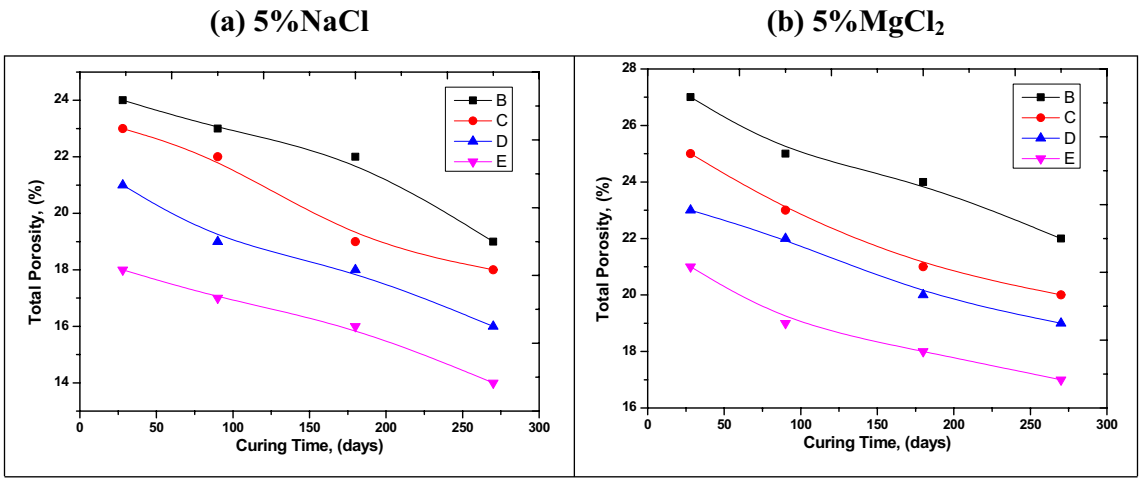

Fig. 6 Total Porosity, (%) of cement pastes as a function of curing time of various proportions of basalt powder in **a** 5%NaCl and **b** $MgCl_2$

filling of space between particles with hydration products, basalt powder additions affect the acceleration of cement hydration, which directly leads to the lowering of capillary pore content [35].

3.1.4 Compressive strength

Tables 10, 11 present the results of compressive strength tests on basalt powder in various proportions that were cured according to ASTM C109 [36] in tap water for up to 28 days (zero time), followed by up to 270 days of immersion in a 5% solution of sodium chloride or magnesium chloride. The results are also shown in Fig. 7, as a function of curing times. The hydration of aluminate, ferro-aluminate, and C3A in addition to the calcium silicate phase is primarily responsible for the increase in strength of the samples with OPC. The hydration product has binder properties while also filling the pores. [37].

During hydration, cement reacts with water to form the two major hydrate phases: calcium silicate hydrate (C–S–H) and calcium hydroxide. The microstructure of the interfacial transition zone (ITZ) largely depends on the way these hydrates are deposited in this zone. At the early stages of hydration, the concentration of silicate ions in solution

Table 10 Compressive strength (kg/cm^2) of cement pastes as a function of curing time of various proportions of basalt powder in 5% NaCl solution

Mix No	Time (days)			
	Compressive strength (kg/cm^2)			
	28 Days	90 Days	180 Days	270 Days
BP0	623	629	644	671
BP5	654	667	689	713
BP10	728	745	756	776
BP20	816	828	864	895

Table 11 Compressive strength (kg/cm^2) of cement pastes as a function of curing time of various proportions of basalt powder in 5% $MgCl_2$ solution

Mix No	Time (days)			
	Compressive strength (kg/cm^2)			
	28 Days	90 Days	180 Days	270 Days
BP0	591	610	624	646
BP5	633	642	681	699
BP10	715	733	742	752
BP20	794	795	817	832

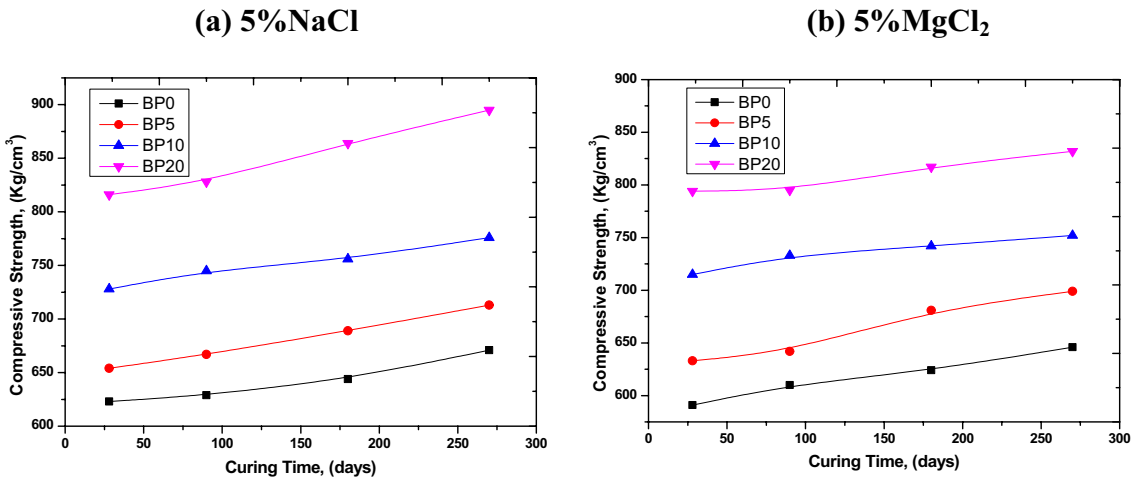

Fig. 7 Compressive strength (kg/cm^2) of cement pastes as a function of curing time of various proportions of Basalt powder in **a** 5%NaCl and **b** $MgCl_2$

is very low, thus the C–S–H phase precipitates mostly around the cement particles. Due to the higher mobility of calcium ions, calcium hydroxide can form in the open pores at a greater distance from cement grains. Furthermore, silica inhibits the nucleation of calcium hydroxide, which favours the precipitation of this phase as far from the cement grains as possible [38].

The pozzolanic characteristics and behaviour of additives play a major role in their chemical reactions. The high alkalinity solution in cement paste dissolves pozzolanically active mineral additions, releasing siliceous ions into the liquid phase [H_3SiO_4]. Both in the paste's pores and on the surface of the mineral additive particles, these ions interact in solution with calcium ions to create a C–S–H phase. Two overlapping phenomena, namely an increase in the effective water/cement ratio and the filling of the pores by hard and high-strength particles of basalt powder, are involved in the physical interaction of basalt powder additions with cement hydration [23].

Basalt's Si–O–Si and Al–O–Si bonds are broken in an alkaline solution by hydroxyl ion, which causes the basalt's alumina silicate network to gradually disintegrate. As the reaction progresses, crystalline and amorphous phases of insoluble oxides and hydroxides are left behind. Under these circumstances, iron hydroxides are essentially insoluble and form corrosion layers on the surface of basalt powder made up of hexagonal plate-like crystals. Because of (i) a very weak bond with the basalt powder and (ii) stress developing in the corrosion shell, the corrosion layer eventually starts to exfoliate. Cement paste surfaces become "fresh" due to the exfoliation of the corrosion shell. The fundamental distinction between etching basalt powder in 5% $MgCl_2$ and 5% NaCl is that the cement pastes degrade to a greater extent in the 5% $MgCl_2$ solution due to the different process rates. This can be explained by the fact that a 5% NaCl solution has a lower concentration of OH ions in saturated solution than a 5% $MgCl_2$ solution [39].

$$2NaCl_{(aq)} + 3CaO \cdot Al_2O_3 \cdot 6H_2O_{(s)} + Ca(OH)_{2(s)} + 4H_2O \rightarrow 3CaO \cdot Al_2O_3 \cdot CaCl_2 \cdot 10H_2O_{(s)} + 2NaOH \quad (4)$$

$$MgCl_{2(aq)} + 3CaO \cdot Al_2O_3 \cdot 6H_2O_{(s)} + Ca(OH)_{2(s)} + 4H_2O \rightarrow 3CaO \cdot Al_2O_3 \cdot CaCl_2 \cdot 10H_2O_{(s)} + Mg(OH)_2 \quad (5)$$

Chloride ions interact with the hydrated and unhydrated phases of cementitious materials when they enter them along with the respective cations (Na^+ and Mg^{2+}). Chloride ions' adsorption on the surface of calcium silicate hydrate (C–S–H) is one of the typical interaction mechanisms between cement paste and chloride for NaCl and $MgCl_2$, respectively. However, it has been noted that concrete exposed to $MgCl_2$ develops an extra potential response in addition to the absorption of chlorides. In the presence of magnesium chloride ($MgCl_2$), cementitious materials undergo reactions with $Ca(OH)_2$ and C–S–H that result in the formation of brucite ($Mg(OH)_2$), calcium oxychloride, and magnesium silicate hydrate (M–S–H), which cause damage and reduce strength. Acoustic emission has been used to find cracks and other damage [40]. With a curing time of up to 360 days and increased lime levels of up to 20 weight percent, the reacted part first increases and

subsequently drops. This is primarily caused by an increase in basalt components' solubility in lime. The rise in alkalinity, which tends to dissolve more of the basalt alumina silicate, may be the cause of the abrupt decline in free lime of 30-wt% lime [41].Silica, alumina, and iron oxide are all common components of pozzolanic materials. When these elements are present in basalt powder, they can react with calcium hydroxide (a byproduct of cement hydration) to form additional calcium silicates hydrate (C–S–H) gel. This reaction increases the strength and durability of the concrete, making it more resistant to chemical attack and improving its long-term performance. Additionally, the presence of silica, alumina, and iron oxide in basalt powder can also contribute to the reduction of calcium hydroxide content in the concrete mixture. This helps to reduce the risk of alkali-silica reaction (ASR) and efflorescence, which can cause deterioration and discoloration of concrete structures over time.

3.2 Characterization of Hydrated pastes mix design

3.2.1 IR spectroscopy

In Fig. 8, the IR spectra of basalt powder in 5% NaCl or $MgCl_2$ at various proportions are displayed. It demonstrates that the sharp band at 3646 cm^{-1} was due to the OH– stretching vibration of calcium hydroxide [42]. The stretching band of H_2O causes a broadband of about 2900–3550 cm^{-1} [43]. The existence of CO_3^{-2}, along with absorption bands at 875 cm^{-1} and 712 cm^{-1} that resulted from the carbonation of portlandite, is responsible for the absorption band at 1418 cm^{-1}. The calcium silicate hydrate (C–S–H) is shown by the band at 970–1100 cm^{-1}. The portlandite band in the mixed cement is more intense at 3646 cm^{-1} than it is in the OPC paste. This is attributed to a couple of factors: first, the dilution effect of the pozzolanic behavior and fillers; second, the pozzolanic reaction of the portlandite brought on by the hydration of the cement phases, which look like pozzolanic phases.

In addition, the asymmetric stretching and vibration bands linked to the Si–O bonds in C–S–H gel units characterise the pattern of the spectrum in the 800–1100 cm^{-1} range [44]. Time, temperature and the presence of pozzolana are the three variables that have an impact on the structure of CSH (Ca/Si). It is believed that when the C–S–H gel is produced during hydration, polymerization linked with that process produces a change in the Si–O stretching vibration to a higher wavenumber as a fingerprint. [45]. Basalt doesn't have thermally unstable minerals. Si–O-Si's asymmetric stretching frequency is responsible for the broadband with a centre frequency of 1,022 cm^{-1}; its symmetric stretching frequency is responsible for the band at 772 cm^{-1}; and its bending frequency is responsible for the band at 452 cm^{-1}.

The characteristic peaks of calcite are disappearing for BP0 and are therefore still present for other samples. These show that what looks like a pozzolanic reaction, or action exchange, devoured all of the lime in the basalt. In addition, the characteristic peaks for CSH sharply appear in the mix of BP20 [46]. Basalt paste showed at 1018 cm^{-1}. The main cause of this variation is cement hydration; larger values are observed to migrate upward, indicating the creation of C–S–H begins at about 966 cm^{-1}. The basalt band Si–O at 1022 cm^{-1} is the alternative weakened and shifted to 1018 cm^{-1}. The breakdown of basalt is intimately tied to this shift. Unreached basalt and the C–S–H band Si–O overlapped and were

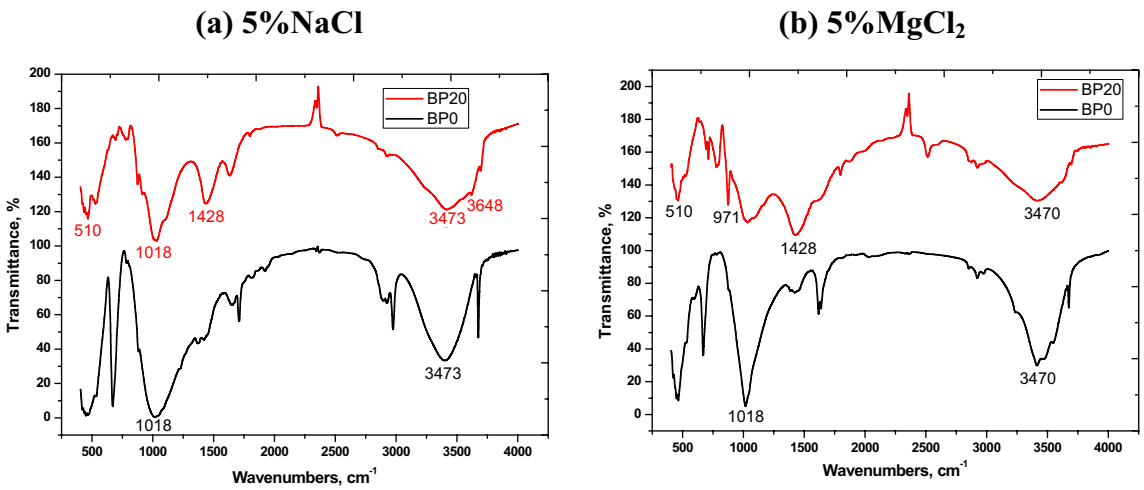

Fig. 8 IR spectra of (0 and 20) wt. % BP in **a** 5%NaCl and **b** $MgCl_2$

centred at 1018 cm^{-1}. Large amounts of CSH are produced by the hydration and pozzolanic reactions that accelerate, changing to greater values [47].

3.2.2 X-ray diffraction (XRD)

X-ray diffraction, which is an approach for figuring out a material's crystal structure, The crystal structure of both the concrete and the basalt powder can be examined using XRD in the case of concrete containing the powder. This can help determine if any compounds or minerals are formed when the two materials are combined; in addition, it can detect any modifications in the concrete's crystal structure brought on by the addition of basalt powder.

XRD of various proportions of basalt powder in 5% NaCl or $MgCl_2$ is shown in Fig. 9. It demonstrated that one of the key hydration products is CH. When basalt was added to the blended cement paste, the peak intensity of $Ca(OH)_2$ dropped. The intensity peaks of $Ca(OH)_2$ appeared at 2 h of 18.07, 34.13, and 47.12.

It is widely known that the amount of $Ca(OH)_2$ consumed in a blended cement paste depends on how much pozzolanic reaction occurs. Fineness and glassy phase content have an impact on the reactivity of pozzolanic materials. Larger and less glassy basalt powders exhibit pozzolanic activity [48]. It could be concluded that basalt has pozzolanic reaction behaviour. During the hydration reaction, basalt interacts with $Ca(OH)_2$ to produce calcium silicate hydrate. This will reduce the pores in crystalline hydration products, uniformize the paste's microstructure, and enhance its durability and impermeability. The service life may be extended as a result of these modifications. Accordingly, basalt is an ideal mineral admixture [48].

BP0 in both media, 5% NaCl and 5% $MgCl_2$ contains (Larnite (Ca_2SiO_4), Portlandite ($Ca(OH)_2$) and Ettringite ($Ca_6Al_2(SO_4)_3(OH)_{12}{\cdot}26H_2O$)) and BP20 contains these compounds in addition to (Calcite($CaCO_3$) and Hatrurite ($Ca_3(SiO_4)O$)) but Labradorite ($Ca0.518Na0.482Al1\ 0.518Si_2{\cdot}482O_8$) is found only in 5% NaCl and Anorthite (Ca, Na)(Si, Al)$4O_8$ is found only in 5% $MgCl_2$.

3.3 Electrochemical impedance spectroscopy (EIS)

Among the different electrochemical techniques that have been extensively developed in the field, electrochemical impedance spectroscopy (EIS) appears to be the most dependable method for observing the corrosion or inhibition processes in reinforced concrete [49].

Without a doubt, water and oxygen are required for the corrosion to proceed in a neutral environment. Normal capillary action allows water to penetrate concrete; the less water that enters the concrete, the slower the rate of oxygen diffusion, and the fewer and smaller the capillary holes are. There are very few H^+ ions to be found in concrete because of its high alkalinity.

Oxygen must be lowered in order to maintain the cathodic reaction since it is consumed in the cathodic reaction. Low water absorptivity and low air void content help prevent chloride ions from penetrating the concrete and contacting the steel's surface [50].

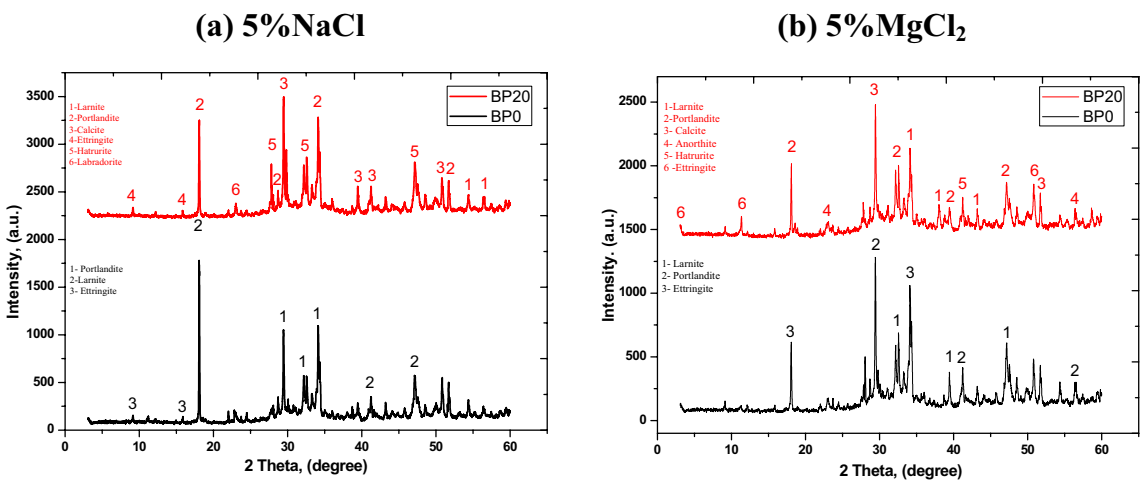

Fig. 9 XRD of BP0 and BP20 in **a** 5%NaCl and **b** $MgCl_2$

This method, in contrast to stationary techniques (the anodic polarization method), enables the non-destructive characterization of both the kinetics of electrochemical reactions that take place on the steel electrode surface and the diffusion of aggressive species within cement-based materials.

Nyquist diagrams of reinforcing steel embedded in different percent basalt powders and immersed in 5% NaCl or $MgCl_2$ for the different periods are shown in Figs. 10 and 11.

According to Tuutti [51], the service life of a concrete structure can be separated into an incubation time (t1) and a propagation period (t2) from the perspective of reinforcement corrosion. The incubation period (t1) relates to the concentration of chloride near the rebar because of its penetration into porous materials. The length of time it takes depends on the concrete cover and the level of chloride necessary to initiate the corrosion process. The propagation time (t2) is the point at which the chloride ions depassivate the surface of the reinforcing steel and start to induce corrosion.

As a result, this adherent surface film demonstrates a decrease in the rate of corrosion of the reinforcing steel. This was demonstrated by the way in which polarization resistance, R_p, changed over time. After a certain amount of time, the system thermodynamically stabilises and Rp achieves a plateau, establishing the combined protection of polarization and alkalinity. Chlorides migrate into the cement-based substance at the same time. Corrosion begins when the chlorides crack the passive coating and get close enough to the reinforcing steel surface to match the threshold value. This alters the electrochemical process (steel with oxygen reduction or anodic oxidation) at the reinforcing steel surface and decreases the Rp value [52–54].

The highest values of R_p were obtained from the BP20 specimen [5% NaCl, R_p equals 807 and 953 Ω cm^2 in 28 days and 270 days], representing the high corrosion resistance, which may be due to binding to the high Al_2O_3 content that leads to the reduction of free chloride in solution. The pozzolanic activity behaviour of basalt powder improved the

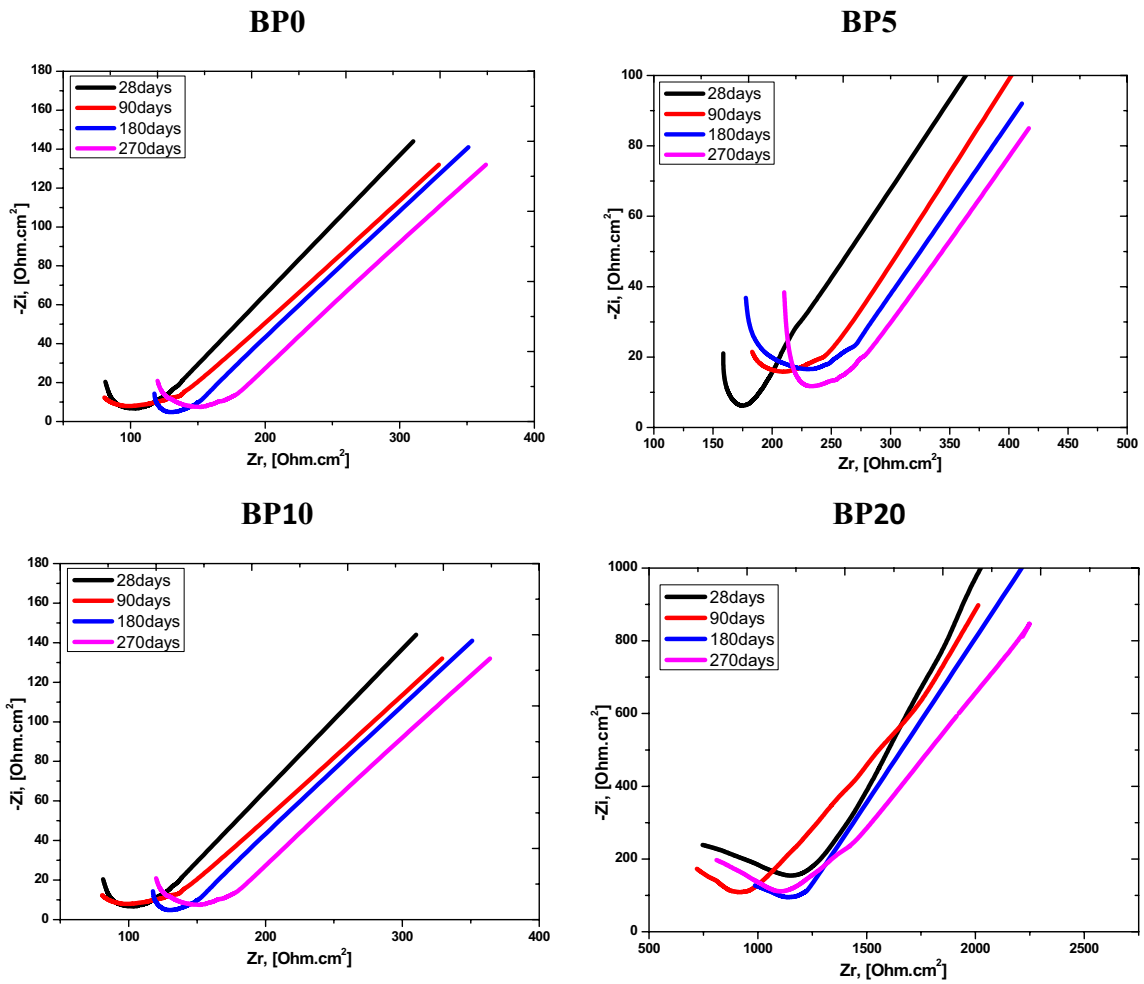

Fig. 10 Nyquist plot of reinforcing steel presented in different proportions of Basalt powder in 5%NaCl

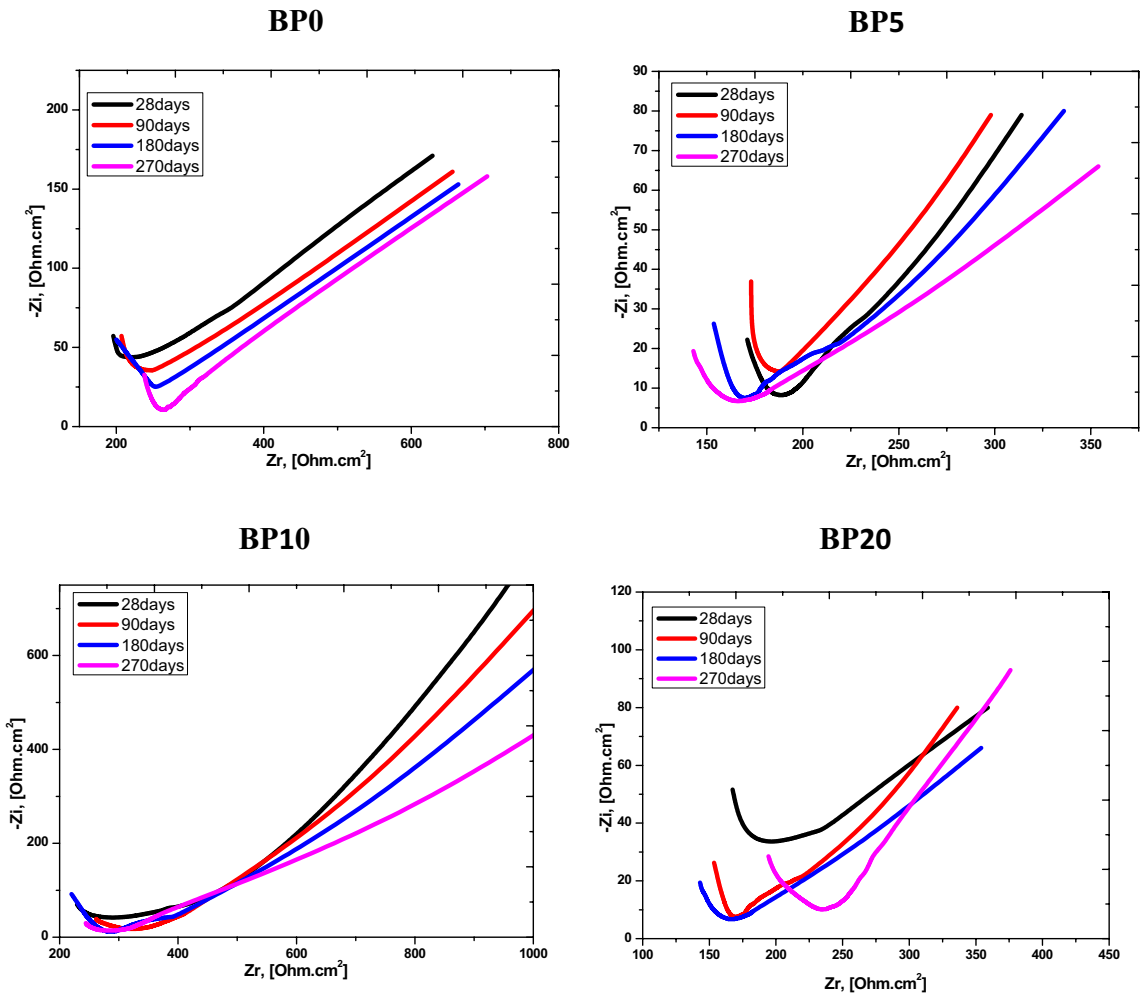

Fig. 11 Nyquist plot of reinforcing steel presented in different proportions of Basalt powder in 5% $MgCl_2$

corrosion resistance of rebar, which appeared from the high values of R_p. The double layer capacitance of reinforcing steel in 5% NaCl (C_{dl}) usually has an opposite R_p trend, in which R_p values have increased due to the improvement of the passive layer and the physical protection by the cement types, C_{dl}, decreased, and vice versa (in 5% NaCl, C_{dl} equals 276 and 129 in 28 days and 270 days).

The values of solution resistance (R_s) increased with time (in 5% NaCl, R_s equals 500 and 596 in 28 days and 270 days) due to the passive layer formation. The R_s in the presence of BP0 get values lower than blended cement specimens (Rs equals 217 and 596 in BP0 and BP20) due to the high degree of permeability in BP0 cement compared with blended cement specimens.

Electrochemical impedance spectroscopy (EIS) measurements come from the following two ideas:

1. The aggressiveness of the $MgCl_2$ solution compared to the NaCl one This behaviour, as mentioned before, is due to the formation of poorly alkaline (pH < 10.4) and insoluble magnesium hydroxide salt as a result of the reaction between magnesium chloride and calcium hydroxide, which reduces the stability of calcium silicate hydrate (C–S–H) and converts it to cohesion-less, porous, reticulated magnesium silicate hydrate (M–S–H) [55]. This is clear from the reduction of R_p values and the increase in C_{dl} values. For all types of concrete specimens immersed in $MgCl_2$ solution compared to NaCl, There is an increase in R_p values with time, as noticed from the low values of R_p [56].
2. Better corrosion protection is provided by plain cement specimens due to the consumption of $Ca(OH)_2$ by the pozzolanic reaction in blend cement specimens, cases where the Mg^{++} cations react directly with the (C–S–H) gel, turning it into the (M–S–H) one [57].

3.4 Spectroscopic analysis

3.4.1 Scanning electron microscopy (SEM)

The examination was carried out on different samples using a VEGA3 TE SCAN (SEM MAG: 500x). The cement matrix that had been combined with the BP had a very solid surface. The hydration of CS resulted in a significant amount of compact calcium hydroxide crystals forming in the voids, indicating that the BP promoted the hydration of concrete and increased the density of the microstructure. Additionally, it agreed with what the XRD had revealed. As a result, BP greatly increased the concrete's strength.

The addition of BP caused the calcium hydroxide crystals to become smaller and more C–S–H gels to form in the concrete, which suggests that BP can further speed up the stage of the concrete's hydration process. To improve the microstructure of the concrete, the calcium hydroxide crystals were further polished. After adding BP, the calcium hydroxide crystals in the concrete were ordered more consistently. It proved that BP was also responsible for the calcium hydroxide's directional arrangement [58].

Figure 12 shows SEM image of the surface of reinforcing steel embedded in BP20 specimens after 270 days of immersion in 5% NaCl and 5% $MgCl_2$. The surface was severely harmed and showed high surface roughness as a result of the aggressiveness of the Mg^{+2} ions in the $MgCl_2$ solution, which changed the C–S–H layer into a cohesion-less porous and reticulated M–S–H layer. However, when NaCl solution is present, there is far less surface damage, which is attributable to the development of a strong protective coating on the rebar surface. The protective film that is created on the surface of the rebar in the 5% NaCl solution seems to be very smooth and completely covers the surface. The ensuing micrographs show that film is forming on the rebar's surface, increasing its resistance. This was due to the BP20 concrete specimens' effective rebar protection. In a study by Song et al. [59], it was shown that BP can interact with $Ca(OH)_2$ crystals to diminish their size and number, densifying the interfacial transition zone (ITZ) of aggregates and cement paste used for binding. The BP particles operate as a nucleus to firmly connect with the CSH-gel particles and fill the spaces in the CSH-gel structure. This indicates that BP treatment decreases the rate at which cement pastes leach calcium, increasing their durability.

3.4.2 Energy dispersive analysis of X-rays (EDX)

C, O, and Fe are confirmed to be important elements by the EDX study. The identification of additional elements includes Mg, Al, S, Na, K, and Ca. According to the SEM analysis of the corrosion state, there are now many more corrosion pits and cracks. The test results demonstrate that the common supplies were widely available in the test samples that were analysed after the half-cell potential test was used to determine the corrosion level. The EDX analysis also confirms the production of Fe_3O_4 in the form of Fe and O for corroded samples of chlorides.

Higher Fe and O are present with less C in the 5% NaCl sample. In comparison to the 5% $MgCl_2$ sample, the same 5% $MgCl_2$ shows a higher C value with less Fe and O. These results were brought about by the addition of basalt powder to the concrete. This will increase corrosion resistance. The BP indeed improved the filling effect in the pore structure

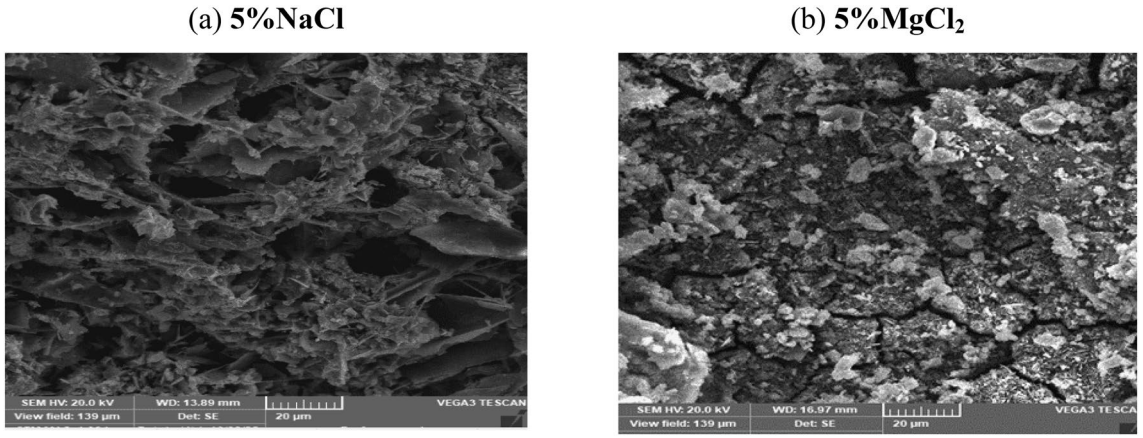

Fig. 12 Surface morphology for reinforcing steel embedded in BP20 paste for 270 days in **a** 5%NaCl and **b** $MgCl_2$

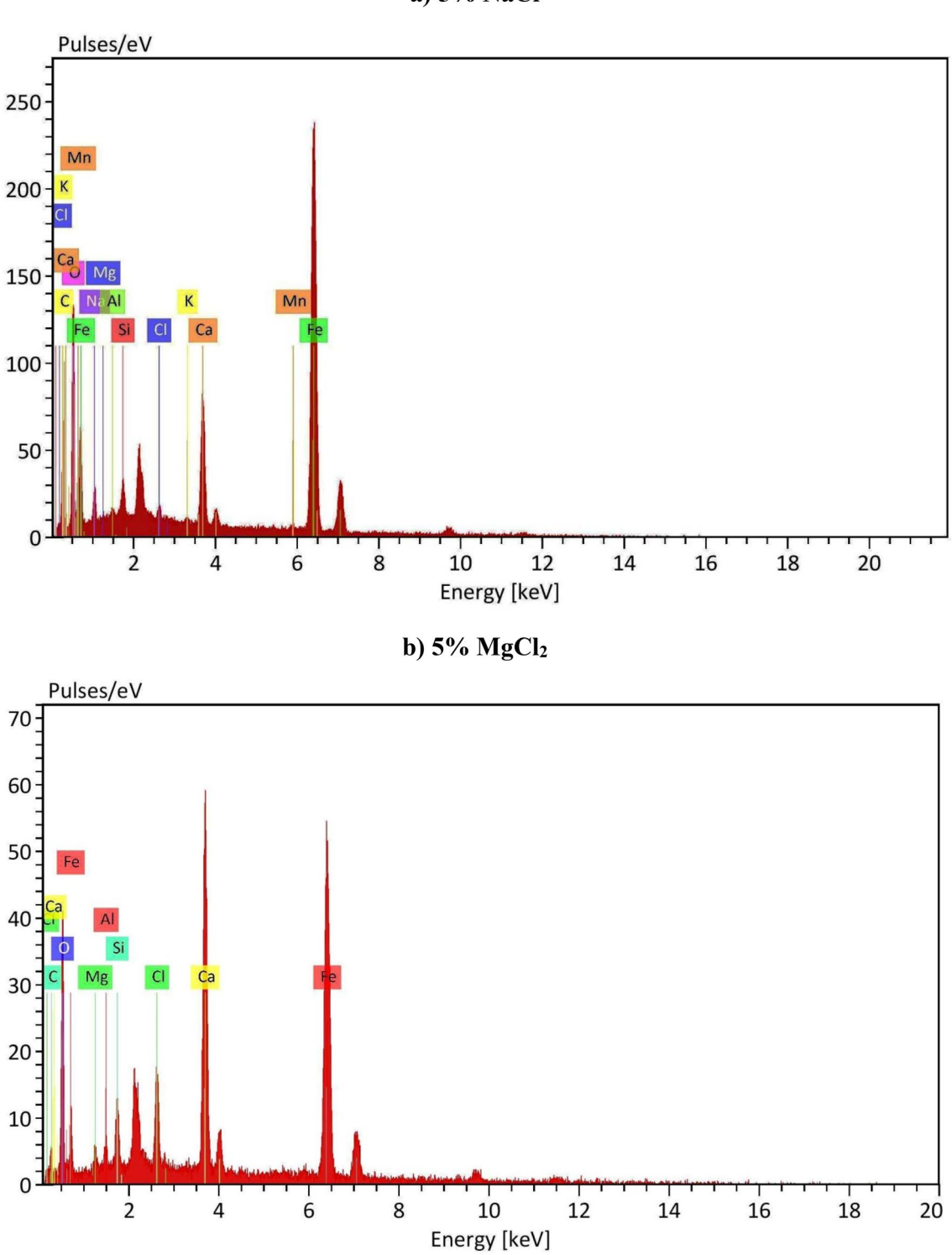

Fig. 13 EDX spectra of the reinforcing steel surface embedded in BP20 paste for 270 days in **a** 5% NaCl and **b** $MgCl_2$

because of the hydration process. This could contribute largely to improving cementitious paste corrosion resistance. It is important to emphasise that the specimens have been shown to have fewer corrosion products and excellent corrosion mitigation capabilities [60].

Table 12 The percentage of elements present on the rebar surface

wt. %	Fe	O	C	Al	Ca	Cl	Si	Mn	Na	K	Mg
5% NaCl	34.41	51.53	9.41	0.16	0.40	3.05	0.37	–	0.95	–	–
5% $MgCl_2$	25.44	43.43	6.55	1.21	15.58	3.92	2.43	–	–	–	1.44

Typical peaks of some of the elements making up the reinforcing steel surface embedded in BP20 specimens after 270 days of immersion in 5% NaCl and 5% $MgCl_2$ are seen in the EDX spectrum in Fig. 13. Table 12 lists the components that are present on the surface of the rebar. The fact that there are fewer Fe bonds in 5% $MgCl_2$ than in 5% NaCl indicates that the protective layer generated on the surface of the rebar provides a high level of protection. Therefore, the results from the electrochemical methods demonstrating the BP20 concrete specimens provide high protection to embedded rebar are supported by the EDX and SEM analyses of reinforcing steel embedded in BP20 concrete specimens and immersed in 5% NaCl and 5% $MgCl_2$ [61].

Based on the previously published data and the currently investigated results, it came to conclude that fine powder addition improved the compressive strength and Physicomechanical characteristics of concrete, confirmed that BP20 has a significant features compared to BP0 [23, 62–69].

4 Conclusion

The following conclusions can be drawn from this work:

1. The compressive strength of cement pastes was improved by addition of basalt powder as a partial replacement (5, 10, and 20%) for cement. The Physicomechanical and physicochemical investigations showed that the basalt powder's addition affects the properties, leading to better particle packing. The large pores in concrete are filled with basalt powder, which improves the mechanical properties of concrete by improving compaction and densifying the structure of the hydrated cement paste.
2. In comparison to concrete without basalt, cement contains basalt powder has a denser and more robust ITZ. This was due to the fact that the basalt powder behaves as a microfilter, which causes the cement matrix surrounding the aggregate particles to physically densify.
3. The hetero-nucleation of the C–S–H phase on the surface of the basalt powder in this area also contributes to the amplification of the ITZ.
4. When comparing BP0 and BP20 in 5% NaCl after 270 days, the partial substitution of cement with BP resulted in a higher compressive strength of 671 and 895 kg/cm^2, respectively. It improves the properties of cement paste and allows a useful and efficient management of industrial wastes.
5. The BP20 specimen in 5% NaCl had the highest values of R_p, 953 ohms cm^2 after 270 days, indicating high corrosion resistance because of binding by high Al_2O_3, which reduces free chloride in solution.
6. The decrease in iron bonds in 5% $MgCl_2$ compared to 5% NaCl showed that a highly adherent protective layer has developed on the surface of the rebar, providing a high level of protection.

Acknowledgements The Academy of Scientific Research and Technology (ASRT) funded this work, through the programme of Scientists for Next Generation (SNG) master scholarship ID: FRM-SGO-22. We would like also to thank Al-Azhar University and National Research Centre for their great support, especially facilities.

Author contributions IAH, GAG and ASA: Suggested the idea, IAH, Performed all experimental work, characterizations and analyses, and wrote the first and second drafts of the manuscript. GAG, ASA, NAG: Supervised the work, revised the the first draft and provided essential corrections and amendements. GAG, ASA NAG: Conceived the content, closely supervised the entire characterization and the experimental work performedin the Lab. NAG Revised and submitted the paper for publication.

Funding This study was funded by the Academy of Scientific Research and Technology (ASRT), Egypt, through the programme of Scientists for Next Generation (SNG) master scholarship ID: FRM-SGO-22. No external funding was used.

Data availability Data is available on request from the authors.

Declarations

Competing interests The authors declare that they have no known competing financial interests or personal relationships that could have appeared to influence the work reported in this paper.

References

1. Ashraf M, Iqbal MF, Rauf M, Ashraf MU, Ulhaq A, Muhammad H, Liu QF. Developing a sustainable concrete incorporating bentonite clay and silica fume: mechanical and durability performance. J Clean Prod. 2022;337: 130315. https://doi.org/10.1016/j.jclepro.2021.130315.
2. Lu M, Xiao H, Liu M, Li X, Li H, Sun L. Improved interfacial strength of SiO_2 coated carbon fibre in cement matrix. Cement Concr Compos. 2018;91:21–8. https://doi.org/10.1016/j.cemconcomp.2018.04.007.
3. Sun H, Zhao D, Gu Y, Memon SA, Ren Z, Liu B, Li D. Three-dimensional characterization of steel corrosion embedded in cement paste. Constr Build Mater. 2017;143:24–32. https://doi.org/10.1016/j.conbuildmat.2017.03.106.
4. Wang L, Chen LT, Sang DC, Guo B, Yang J, Shen Z, Poon CS. Biochar as green additives in cement-based composites with carbon dioxide curing. J Clean Prod. 2020;258: 120678. https://doi.org/10.1016/j.jclepro.2020.120678.
5. Saraya ME. Study physico-chemical properties of blended cements containing fixed amount of silica fume, blast furnace slag, basalt and limestone, a comparative study. Constr Build Mater. 2014;72:104–12. https://doi.org/10.1016/j.conbuildmat.2014.08.071.
6. Alla S, Jayaram M, Asadi SS. An experimental investigation for replacements of river sand and cement with Robosand, fly-ash and silica fume in concrete to evaluate the influence in durability properties. Mater Today Proc. 2021;43:954–61. https://doi.org/10.1016/j.matpr.2020.07.340.
7. Siddique R, Klaus J. Influence of metakaolin on the properties of mortar and concrete: a review. Appl Clay Sci. 2009;43(3–4):392–400. https://doi.org/10.1016/j.clay.2008.11.007.
8. Martinez-Reyes J, Alavez-Ramírez R, Montes-García P, Jiménez-Quero V. Mineralogical effect on the pozzolanic reactivity of a Mexican lacustrine soil. Constr Build Mater. 2010;24(12):2650–7. https://doi.org/10.1016/j.conbuildmat.2010.04.059.
9. Rahhal V, Bonavetti V, Trusilewicz L, Pedrajas C, Talero R. Role of the filler on Portland cement hydration at early ages. Constr Build Mater. 2012;27(1):82–90. https://doi.org/10.1016/j.conbuildmat.2011.07.021.
10. Jain N. Effect of nonpozzolanic and pozzolanic mineral admixtures on the hydration behavior of ordinary Portland cement. Constr Build Mater. 2012;27(1):39–44. https://doi.org/10.1016/j.conbuildmat.2011.08.006.
11. Ghanem WA, Ghayad IM, Gaber GA. Corrosion behavior of reinforcing steel in cement partially replaced with metakaolin in 3.5% NaCl and 5% MgSO4 solutions. Int J Metal Mater Sci Eng. 2013;3(5):1–8.
12. Ahmed ASI, Ghanem WA, El-shenawy AE, Hussein WA, Gaber GA. Physico-mechanical properties of blended slag cement and plain cement in 5% sodium sulphate solution. Int J Metal Mater Sci Eng. 2016;6(2):7–16.
13. Lachemi M, Hossain KM, Lambros V, Nkinamubanzi PC, Bouzoubaâ N. Self-consolidating concrete incorporating new viscosity modifying admixtures. Cem Concr Res. 2004;34(6):917–26. https://doi.org/10.1016/j.cemconres.2003.10.024.
14. Lian H, Lu X. Principles and methods of high performance concrete design according to durability requirement. Architecture. 2001;1:8–11.
15. Fu Q, Xu W, Bu M, Guo B, Niu D. Orthogonal experimental study on hybrid-fiber high-durability concrete for marine environment. J Market Res. 2021;13:1790–804. https://doi.org/10.1016/j.jmrt.2021.05.088.
16. Adesina A. Performance of cementitious composites reinforced with chopped basalt fibres–an overview. Constr Build Mater. 2021;266: 120970. https://doi.org/10.1016/j.conbuildmat.2020.120970.
17. Yang L, Xie H, Zhang D, Zhang F, Lin C, Fang S. Acoustic emission characteristics and crack resistance of basalt fiber reinforced concrete under tensile load. Constr Build Mater. 2021;312: 125442. https://doi.org/10.1016/j.conbuildmat.2021.125442.
18. Li J, Che D, Liu Z, Yu L, Ouyang X. Effect of basalt powder on hydration, rheology, and strength development of cement paste. Materials. 2022;15(23):8632. https://doi.org/10.3390/ma15238632.
19. Assie S, Escadeillas G, Waller V. Estimates of self-compacting concrete 'potential'durability. Constr Build Mater. 2007;21(10):1909–17. https://doi.org/10.1016/j.conbuildmat.2006.06.034.
20. Unčík S, Kmecová V. The effect of basalt powder on the properties of cement composites. Procedia Eng. 2013;65:51–6. https://doi.org/10.1016/j.proeng.2013.09.010.
21. Topcu IB, Bilir T, Uygunoğlu T. Effect of waste marble dust content as filler on properties of self-compacting concrete. Constr Build Mater. 2009;23(5):1947–53. https://doi.org/10.1016/j.conbuildmat.2008.09.007.
22. Tasong WA, Cripps JC, Lynsdale CJ. Aggregate-cement chemical interactions. Cem Concr Res. 1998;28(7):1037–48. https://doi.org/10.1016/S0008-8846(98)00067-2.
23. Laibao L, Yunsheng Z, Wenhua Z, Zhiyong L, Lihua Z. Investigating the influence of basalt as mineral admixture on hydration and microstructure formation mechanism of cement. Constr Build Mater. 2013;48:434–40. https://doi.org/10.1016/j.conbuildmat.2013.07.021.
24. Yu R, Spiesz PH, Brouwers HJ. Development of an eco-friendly Ultra-High Performance Concrete (UHPC) with efficient cement and mineral admixtures uses. Cement Concr Compos. 2015;55:383–94. https://doi.org/10.1016/j.cemconcomp.2014.09.024.

25. Youness D, Mechaymech A, Al Wardany R. Flow assessment and development towards sustainable self-consolidating concrete using blended basalt and limestone-cement systems. J Clean Prod. 2021;283: 124582. https://doi.org/10.1016/j.jclepro.2020.124582.
26. Li L, Nam J, Hartt WH. Ex situ leaching measurement of concrete alkalinity. Cem Concr Res. 2005;35(2):277–83. https://doi.org/10.1016/j.cemconres.2004.04.024.
27. Dobiszewska M, Schindler AK, Pichór W. Mechanical properties and interfacial transition zone microstructure of concrete with waste basalt powder addition. Constr Build Mater. 2018;177:222–9. https://doi.org/10.1016/j.conbuildmat.2018.05.133.
28. Kılıç A, Atiş CD, Teymen A, Karahan OK, Özcan F, Bilim C, Özdemir ME. The influence of aggregate type on the strength and abrasion resistance of high strength concrete. Cement Concr Compos. 2008;30(4):290–6. https://doi.org/10.1016/j.cemconcomp.2007.05.011.
29. Davraz M, Ceylan H, Topçu İB, Uygunoğlu T. Pozzolanic effect of andesite waste powder on mechanical properties of high strength concrete. Constr Build Mater. 2018;165:494–503. https://doi.org/10.1016/j.conbuildmat.2018.01.043.
30. Tantawi SH, Selim IZ. Improvement of concrete properties and reinforcing steel inhibition using a natural product admixture. J Mater Sci Technol. 1996;12(2):95.
31. Khater HM. Effect of calcium on geopolymerization of aluminosilicate wastes. J Mater Civ Eng. 2012;24(1):92–101. https://doi.org/10.1061/(ASCE)MT.1943-5533.0000352.
32. ASTM C140/C140M. Standard test method for sampling and testing concrete masonry units and related units. West Conshohocken: American Society for Testing and Materials; 2015.
33. Kočí V, Vejmelková E, Koňáková D, Pommer V, Grzeszczyk S, Matuszek-Chmurowska A, Černý R. Basic physical, mechanical, thermal and hygric properties of reactive powder concrete with basalt and polypropylene fibers after high-temperature exposure. Constr Build Mater. 2023;374: 130922. https://doi.org/10.1016/j.conbuildmat.2023.130922.
34. Kiran T, Andrushia D, El Hachem C, Kanagaraj B, Anand N, Azab M. Effect of nano cementitious composites on corrosion resistance and residual bond strength of concrete. Results in Engineering. 2023;18: 101064. https://doi.org/10.1016/j.rineng.2023.101064.
35. Topçu İB, Uygunoğlu T. Effect of aggregate type on properties of hardened self-consolidating lightweight concrete (SCLC). Constr Build Mater. 2010;24(7):1286–95. https://doi.org/10.1016/j.conbuildmat.2009.12.007.
36. ASTM C109/C109M. Standard test method for compressive strength of hydraulic cement mortars (using2-in. or [50-mm] cube specimens). West Conshohocken: American Society for Testing and Materials; 2013.
37. Dobiszewska M. Waste materials used in making mortar and concrete. J Mater Educ. 2017;39(5–6):133–56.
38. Scrivener KL, Crumbie AK, Laugesen P. The interfacial transition zone (ITZ) between cement paste and aggregate in concrete. Interface Sci. 2004;12:411–21. https://doi.org/10.1023/B:INTS.0000042339.92990.4c.
39. Yong-Sik Y, Hwa-Sung R, Hee-Seob L, Kyung-Taek K, Jeong-Su K, Seung-Jun K. Effect of grout conditions and tendon location on corrosion pattern in PS tendon in grout. Constr Build Mater. 2018;186:1005–15. https://doi.org/10.1016/j.conbuildmat.2018.08.023.
40. Pruckner F, Gjørv OE. Effect of $CaCl_2$ and NaCl additions on concrete corrosivity. Cem Concr Res. 2004;34(7):1209–17. https://doi.org/10.1016/j.cemconres.2003.12.015.
41. De Melo CV, Gomes PC, Moraes KA. A study of packing parameters that influence the fresh properties of self-compacting concrete. Cerâmica. 2019;65:432–42. https://doi.org/10.1590/0366-69132019653752667.
42. Gleize PJ, Motta EV, Silva DA, Roman HR. Characterization of historical mortars from Santa Catarina (Brazil). Cement Concr Compos. 2009;31(5):342–6. https://doi.org/10.1016/j.cemconcomp.2009.02.013.
43. Rybin VA, Utkin AV, Baklanova NI. Corrosion of uncoated and oxide-coated basalt fibre in different alkaline media. Corros Sci. 2016;102:503–9. https://doi.org/10.1016/j.corsci.2015.11.004.
44. Mollah MY, Yu W, Schennach R, Cocke DL. A Fourier transform infrared spectroscopic investigation of the early hydration of Portland cement and the influence of sodium lignosulfonate. Cem Concr Res. 2000;30(2):267–73. https://doi.org/10.1016/S0008-8846(99)00243-4.
45. Ylmén R, Jäglid U, Steenari BM, Panas I. Early hydration and setting of Portland cement monitored by IR, SEM and Vicat techniques. Cem Concr Res. 2009;39(5):433–9. https://doi.org/10.1016/j.cemconres.2009.01.017.
46. Dobiszewska M, Beycioğlu A. Physical properties and microstructure of concrete with waste basalt powder addition. Materials. 2020;13(16):3503.
47. Zhang P, Zuo Y. Relationship between porosity, pore parameters and properties of microarc oxidation film on AZ91D magnesium alloy. Results Phys. 2019;12:2044–54. https://doi.org/10.1016/j.rinp.2019.01.095.
48. Moropoulou A, Bakolas A, Anagnostopoulou S. Composite materials in ancient structures. Cement Concr Compos. 2005;27(2):295–300. https://doi.org/10.1016/j.cemconcomp.2004.02.018.
49. Yalçin H, Koç T. Solar power for cathodic protection of steel pipeline. Sol Energy. 1993;51(5):415–8. https://doi.org/10.1016/0038-092X(93)90155-H.
50. Ghanem WA, Ahmed AS, El-Shenawy AE, Hussein WA, Gaber GA. Mechanical properties and corrosion behavior of reinforcing steel in different cement with addition of nano-silica on blended cement in tap water. J Civil Eng. 2016;1(1):13–34. https://doi.org/10.3390/ma13163503.
51. Tuutti K. Service life of structures with regard to corrosion of embedded steel. Special Publ. 1980;65:223–36. https://doi.org/10.14359/6355.
52. Dobiszewska M, Pichór W, Szołdra P. Effect of basalt powder addition on properties of mortar. In MATEC Web Conf. 2019;262:6002. https://doi.org/10.1051/matecconf/201926206002.
53. Yu H, Meng T, Zhao Y, Liao J, Ying K. Effects of basalt fiber powder on mechanical properties and microstructure of concrete. Case Stud Constr Mater. 2022;17:01286. https://doi.org/10.1016/j.cscm.2022.e01286.
54. -Asrar N, Malik AU, Ahmad S, Andijani IN corrosion protection of rebars in concretes. In: Second acquired experience symposium on desalinisation plants O&M, SWCC, Al-Jubail, Sept. p. 1456–77
55. Poupard O, Aıt-Mokhtar A, Dumargue P. Corrosion by chlorides in reinforced concrete: Determination of chloride concentration threshold by impedance spectroscopy. Cem Concr Res. 2004;34(6):991–1000. https://doi.org/10.1016/j.cemconres.2003.11.009.
56. Buyuksagis IS, Uygunoglu T, Tatar E. Investigation on the usage of waste marble powder in cement-based adhesive mortar. Constr Build Mater. 2017;154:734–42. https://doi.org/10.1016/j.conbuildmat.2017.08.014.

57. Martirena, JF, Day RL, Middendorf B., Gehrke M, Martínez L, Dopico JM. Lime-pozzolan binder as a very fine mineral admixture in concrete. In: Proceedings of the international symposium on ultra high performance concrete; 2004. (3): 117–31.
58. Liu H, Lyu X, Zhang Y, Luo G, Li W. Steel corrosion evaluation of basalt fiber RPC affected by crack and steel-concrete interface damage using electrochemical methods. Sensors. 2020;20(18):5027.
59. Song Z, Jiang L, Chu H, Xiong C, Liu R, You L. Modeling of chloride diffusion in concrete immersed in CaCl2 and NaCl solutions with account of multi-phase reactions and ionic interactions. Constr Build Mater. 2014;66:1–9. https://doi.org/10.1016/j.conbuildmat.2014.05.026.
60. Huzni S, Ibrahim IB, Fonna S, Pidaparti R. Physics-based surrogate model for reinforced concrete corrosion simulation. Results Eng. 2022;16: 100659. https://doi.org/10.1016/j.rineng.2022.100659.
61. Rybin VA, Utkin AV, Baklanova NI. Alkali-resistant coating for basalt fibers. Prot Met Phys Chem Surf. 2013;49:689–92. https://doi.org/10.1134/S2070205113060142.
62. Van Oss HG, Padovani AC. Cement manufacture and the environment part II: environmental challenges and opportunities. J Ind Ecol. 2003;7(1):93–126. https://doi.org/10.1162/108819803766729212.
63. Uzal B, Turanli L, Mehta PK. High-volume natural pozzolan concrete for structural applications. ACI Mater J. 2007;104(5):535. https://doi.org/10.14359/18910.
64. Constantiner D, Diamond S. Alkali release from feldspars into pore solutions. Cement Concr Res. 2003;33(4):549–54. https://doi.org/10.1016/S0008-8846(02)01001-3.
65. Uysal M, Yilmaz K. Effect of mineral admixtures on properties of self-compacting concrete. Cement Concr Compos. 2011;33(7):771–6. https://doi.org/10.1016/j.cemconcomp.2011.04.005.
66. Saraya ME. Study the pozzolanic activity of fresh basalt. J Mater Sci Eng. 2011;A1(6A):790.
67. Grzeszczyk S, Starzyk, K. Importance of cement type in the microstructure of interfacial transition zone in HPC. Cement Wapno Beton; 2004
68. Kong L, Du Y. Interfacial interaction of aggregate-cement paste in concrete. J Wuhan Univ Technol Mater Sci Ed. 2015;30(1):117–21. https://doi.org/10.1007/s11595-015-1111-z.
69. Bonavetti VL, Rahhal VF, Irassar EF. Studies on the carboaluminate formation in limestone filler-blended cements. Cement Concr Res. 2001;31(6):853–9. https://doi.org/10.1016/S0008-8846(01)00491-4.